Analysis and design of antithetic proportional-integral-derivative biocontrol-systems with species dilution

Xun Deng [a], Hui Lv [a,*], Qiang Zhang [a], Edmund Ming Kit Lai [b]

[a] Key Laboratory of Advanced Design and Intelligent Computing, School of Software Engineering, Dalian University, Dalian 116622, Liaoning, China
[b] School of Engineering, Computer and Mathematical Sciences, Auckland University of Technology, Auckland 1010, New Zealand

ARTICLE INFO

Keywords:
Antithetic PID controller
Robust perfect adaptation
Degradation inhibition mechanism
Species dilution
BCRNs

ABSTRACT

The nonlinearity and non-separability of the antithetic PID (aPID) controller have provided greater flexibility in the design of biochemical reaction networks (BCRNs), resulting in significant impacts on biocontrol-systems. Nevertheless, the dilution of control species is disregarded in designs of aPID controllers, which would lead to the failure of inhibition mechanism in the controller and loss of robust perfect adaptation (RPA)—the biological counterpart of robust steady-state tracking. Here, the impact of dilution processes on the structure of aPID is investigated in this study. It is discovered that the proportional and low-pass filters are altered when the dilution processes is present in control species, which increases the coupling between the controller parameters. Moreover, additional integrations for the reference signal and control output generated by control species dilution further leads to the loss of RPA. Subsequently, a novel aPID controller represented by BCRNs, termed quasi-aPID, has been designed to eliminate the detrimental effects of the dilution processes. In an effort to ameliorate the interdependencies among controller parameters, a degradation inhibition mechanism is employed within this controller. Furthermore, this work establishes the limiting relationship between the controller's reaction rates in order to guarantee RPA, while abstaining from the introduction of supplementary species and biochemical reactions. By using the quasi-aPID controller in both the Escherichia coli gene expression model and the whole-body cholesterol metabolism model, its effectiveness is confirmed. Simulation results demonstrate that, the quasi-aPID exhibits a smaller absolute steady-state error in both models and guarantees the RPA property.

1. Introduction

One of the fundamental characteristics of biological systems is their ability to maintain stability in the uncertain external environment, which is typically achieved through endogenous feedback regulatory mechanisms [1–3]. Restoring internal balance when endogenous regulatory mechanisms fail has been a focus of researchers [4,5]. Fortunately, the rational design of biomolecular feedback controllers holds promise for addressing this issue [6–9].

The integral controller ensures that the system's output approaches the desired reference signal and perfectly adapts to disturbances, a property known as robust steady-state tracking or robust perfect adaptation in the biological context [10–12]. Moreover, the integral controller has strong scalability and flexibility, as it can be transformed into a proportional–integral (PI) controller or a proportional–integral–derivative (PID) controller by incorporating proportional and derivative modules [13–15]. However, there are several limitations in implementing PID controllers using biomolecules. Firstly, BCRNs inherently possess nonlinear structures [16,17]. Secondly, the quantities of the controlled objects, such as protein copy numbers or concentrations, cannot be negative. To achieve RPA, researchers initially focused on implementing independent integral controllers [18–20]. Subsequently, a series of aPI and aPID controllers have been proposed to enhance control performance while ensuring RPA. Unlike other molecular PID controllers, the aPID controller is based on antithetic motif, with the reference signal defined by the reaction rate of the reference reaction and the control output defined by the reaction rate of the controller reactions. In contrast to molecular PID controllers which not based on antithetic motif, the control output is set based on the concentration of the control species, aPID controllers typically exhibit fewer species and reactions [21,22]. The biological implementation of aPID controllers requires the design of mechanisms that facilitate the adjustable modulation of reaction rates. This is often achieved through specific activators, inhibitors, or the design of specific binding sites on the control species [17,23].

* Corresponding author.
E-mail addresses: dengxun@s.dlu.edu.cn (X. Deng), lh8481@tom.com (H. Lv), zhangq@dlu.edu.cn (Q. Zhang), edmund.lai@aut.ac.nz (E.M.K. Lai).

The antithetic motif is essential for achieving RPA [24]. Based on the antithetic motif, the antithetic integral (aI) controller is proposed [10,19]. Studies on implementing the aI controller in cells have identified that the dilution of the controlled species, synchronized with cell growth, disrupts the functionality of the aI controller, and corresponding solutions have been proposed [19,24]. Building upon the aI controller, a design method for the aPID controller has been proposed [17]. Compared to previously proposed biomolecular PID controllers, the aPID controller is more suitable for implementation using BCRNs and involves fewer reactions and control species. Previous studies are influenced by the design of traditional PID controllers, focusing on separately implementing the P, I, and D components and then summing them together, assuming linear dynamics of the controller [22,25,26]. However, the feedback mechanisms in BCRNs are inherently nonlinear, and there is no reason to constrain the dynamics of the controller to be linear [17]. Moreover, these controller designs introduce additional species, increasing the complexity of their biological implementation. The aPID controller is a nonlinear controller, and its P, I, and D components are not independent. Researches have shown that aPID possesses several excellent characteristics, including but not limited to guaranteeing RPA, enhancing stability, and dynamic performance [9,17,23].

In living systems, widespread inhibitory mechanisms are critical for maintaining system homeostasis [27,28], and the aPID controller is formed by introducing an inhibitory mechanism based on the antithetic motif [17]. Different types of inhibitory mechanisms can result in aPID controllers with different performance characteristics. According to the study in Ref. Filo et al. [17], aPID controllers utilizing degradation inhibition exhibit more prominent performance. In the biochemical implementation of non-antithetic feedback controllers, time-delay and leakage reactions are important issues to consider [29–32]. While controlling the dilution of species is a more urgent problem to be solved in the design of antithetic feedback controllers [17,19]. Because whether it is the natural degradation of the control species, or the change of environment in which the controller is located, such as the growth and division of cells, will lead to the dilution of the control species [17], which in turn will lead to the failure of the antithetic motif in the antithetic feedback controller. Nevertheless, the existence of species dilution is disregarded in earlier aPID controller designs. Therefore, while aPID controller may be able to provide the intended control function in cell-free environments without causing natural species degradation theoretically, our simulated results show that the RPA is not maintained when molecular dilution is present. It should be noted that earlier research on species dilution in controllers is limited to aI controllers. This is because the molecular dilution problem in the aPID controller is much more complex than the dilution problem in the aI controller. In actuality, the molecular dilution problem in aPID controllers cannot be solved by the usual strategy for addressing molecular dilution in aI controllers because of inhibition mechanism.

In this work, investigations are conducted into the causes of the loss of RPA characteristics in aPID controllers when control species dilution is present. Furthermore, a new aPID controller, namely quasi-aPID, is designed to mitigate the detrimental effects caused by control species dilution. Specifically, a mathematical method is used to create the controller in the presence of dilution and to determine the precise limiting relationships that the reaction rates of the various reactions within the controller needed to satisfy. By following this method, the scope of applicability for quasi-aPID is clearly defined. Importantly, these conditions hold true under mild assumptions and are largely independent of specific parameter values. Then the effectiveness of the quasi-aPID design is validated through numerical simulations conducted on two typical models in synthetic biology, namely the gene expression model in Escherichia coli and the whole-body cholesterol metabolism model.

This study elucidates the impact of species dilution process on the structure of aPID controller, and theoretically explains the reason behind the loss of RPA property of aPID controller. The newly designed quasi-aPID overcomes the detrimental effects of species dilution, facilitating the application of aPID controller in a wider range of biological fields such as implementing quasi-aPID in rapidly proliferating cells. Moreover, quasi-aPID enriches the types of aPID controllers and provides a valuable reference for designing other types of aPID controllers with dilution processes.

2. Impact analysis of species dilution on the structure of aPID controller

In this section, the BCRNs of aPID with dilution processes are described. A comprehensive explanation of the species and related biochemical reactions is provided, along with the dynamic model of the closed-loop system consisting of the controlled network and the aPID controller. Subsequently, the closed-loop system undergoes linearization using the linear perturbation approach. Structural block diagrams of the controller are obtained for both scenarios, with and without dilution of the control species. These diagrams form the basis for a study examining the impact of dilution processes on the aPID controller's control capability.

2.1. Symbol description

Block diagrams are typically used to describe feedback control systems. However, this research adopts a general framework proposed in [17] to adjust to the biological situation. The control and the controlled network, or the controller and plant, are described by BCRNs.

Consider a general plant shown in Fig. 1 in orange. This network has n species $X := \{X_1, \dots, X_n\}$, each of which reacts with m reaction channels, represented by $R := \{R^1, \dots, R^m\}$. Every reaction $R^i (i = 1, \dots, m)$ has a propensity function $\lambda_i : \mathbb{R}_+^m \to \mathbb{R}_+$ and a stoichiometric vector $\zeta_i \in \mathbb{Z}^{n\times 1}$. The combination of the propensity function (vector-valued) $\lambda := \begin{bmatrix}\lambda_1 & \lambda_2 & \dots & \lambda_m\end{bmatrix}^T$, species X, and stoichiometric matrix $S := \begin{bmatrix}\zeta_1 & \zeta_2 & \cdots & \zeta_m\end{bmatrix} \in \mathbb{Z}^{n\times m}$ can characterize a controlled network, denoted as $\mathrm{N} := (X, S, \lambda)$, which is also referred to as an open-loop system. Using the catalytic reaction $A \xrightarrow{\tau} A + B$ as an example, the stoichiometric vector is $\begin{bmatrix}0 & 1\end{bmatrix}^T$, the propensity function is τa, where A and B are species, a is the concentration of the species A, τ is the reaction rate.

The aim of this study is to construct a controller N_c, or control network, that has the ability to regulate the concentration of X_n within the regulated network N. With the exception of species X_1 and X_n, it is presumed that the controller cannot access any other species within the controlled network. To be more precise, the controller "senses" the control network's output species X_n, "processes" the sensed signal via the control species $Z := \{Z_1, Z_2\}$, and then "actuates" the regulated network's input species X_1. The control species are permitted to interact with the plant input/output species as well as with one another through l reaction channels, represented by $\mathcal{R}_c := \{\mathcal{R}_c^1, \mathcal{R}_c^2, \dots, \mathcal{R}_c^l\}$. Let $\bar{S}_c \in \mathbb{Z}^{4\times l}$ and $\lambda_c : \mathbb{R}_+^4 \to \mathbb{R}_+^l$ denote the stoichiometry matrix and propensity function of the controller, respectively.

The stoichiometry matrix $\bar{S}_c$ can be partitioned as $\bar{S}_c := [S_1 S_n S_c]$ because the controller reactions R_c involve the controller species Z and the plant input/output species X_1/X_n. We assume that the output increases with an increase in the input. Here, the stoichiometry coefficients of the plant input and output species X_1 and X_n, respectively, among the controller reaction channels R_c are encrypted by the two variables, S_1 and S_n. Moreover, the controller species' stoichiometry coefficients are encrypted by S_c. Therefore, designing S_1, S_n, S_c, and λ_c is the main task involved in the controller design problem. Take note that we only include plants with single-input, single-output species for simplicity's sake. But by adding more rows to S_1 and S_n, this may be easily adapted to multiple-input-multiple-output species. In the end, the closed-loop system consists of the open-loop network enhanced with the controller network, encompassing all the species of plants and controllers $X_{cl} := X \cup Z$ and reactions $R_{cl} := R \cup R_c$. The propensity function λ_{cl} and closed-loop stoichiometry matrix S_{cl} together can therefore fully represent the closed-loop network, $\mathrm{N_{cl}} := \mathrm{N} \cup \mathrm{N_c}$.

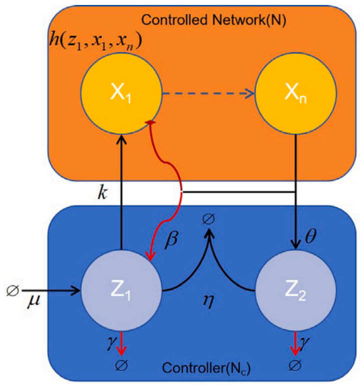

$$S_{cl} := \begin{array}{c} \left[\begin{array}{c|cccccc} & 0 & 1 & 0 & 0 & 0 & 0 \\ S & & & & 0 & & \\ & 0 & 0 & 0 & 0 & 0 & 0 \\ \hline 0 & 1 & 0 & 0 & 1 & 1 & 0 \\ & 0 & 0 & 1 & 1 & 0 & 1 \end{array}\right] \end{array} \begin{array}{l} S_1 \\ \\ S_n \\ S_c \\ \end{array}$$

$$\lambda_{cl}(x,z) = \left[\lambda^T(x) \quad | g(\mu, x_n) \quad h(z_1, x_1, x_n) \quad \theta x_n \quad \eta z_1 z_2 \quad \gamma z_1 \quad \gamma z_2\right]^T$$

Fig. 1. Closed-loop system composed of the aPID controller with dilution and plant.

Table 1
The BCRNs of aPID.

Reaction name	BCRN	Propensity function	Stoichiometry vector
Reference Rxn: R_r	$\emptyset \xrightarrow{g} Z_1$	$g(\mu, x_n)$	$[0 \cdots 0\ 1\ 0]^T$
Actuation Rxn: R_a	$\emptyset \xrightarrow{h} X_1$	$h(z_1, x_1, x_n)$	$[1 \cdots 0\ 0\ 0]^T$
Sensing Rxn: R_s	$X_n \xrightarrow{\theta} X_n + Z_2$	θx_n	$[0 \cdots 0\ 0\ 1]^T$
Sequestration Rxn: R_q	$Z_1 + Z_2 \xrightarrow{\eta} \emptyset$	$\eta z_1 z_2$	$[0 \cdots 0\ -1\ -1]^T$
Dilution Rxn1: R_{d_1}	$Z_1 \xrightarrow{\gamma} \emptyset$	γz_1	$[0 \cdots 0\ -1\ 0]^T$
Dilution Rxn2: R_{d_2}	$Z_2 \xrightarrow{\gamma} \emptyset$	γz_2	$[0 \cdots 0\ 0\ -1]^T$

2.2. Controller description

An incoherent feedforward loop (IFFL) and an antithetic motif are the two main components of an aPID. In Fig. 1, the reactions in the IFFL are indicated by red lines, whereas the reactions in the antithetic motif are depicted by black lines. For every reaction, Table 1 displays the stoichiometry vector, propensity function, and BCRN representation.

To be specific, R_r represents the reference reaction, which is equivalent to $\emptyset \xrightarrow{\mu} Z_1$ and $X_n \xrightarrow{\beta} X_n + Z_1$, thus $g(\mu, x_n) = \mu + \beta x_n$. More precisely, $\emptyset \xrightarrow{\mu} Z_1$ belongs to the antithetic motif, while $X_n \xrightarrow{\beta} X_n + Z_1$ belongs to the IFFL. R_a is the "driving" reaction that implements the controller's actuaion on the plant, its propensity function depends on the specific inhibition mechanism. When there is no inhibitory reaction present, the given reaction is equivalent to $Z_1 \xrightarrow{k} Z_1 + X_1$, thus $h(z_1, x_1, x_n) = kz_1$, and it serves as the driving force within the antithetic motif. However, when inhibitory reaction is present, it interacts with $X_n \xrightarrow{\beta} X_n + Z_1$ to form a complete IFFL. Specifically, the inhibition mechanism can be described as the output X_n directly inhibits the input X_1 and simultaneously produces it via the intermediate species Z_1. R_s is the measurement reaction, where the concentration change of controlled species X_n is reflected by the concentration change of control species Z_2; R_q is the sequestration reaction, which associates control species Z_1 and Z_2 to prevent unbounded growth of the control species. $\emptyset \xrightarrow{\mu} Z_1$, $Z_1 \xrightarrow{k} Z_1 + X_1$, R_s and R_q combine to form the antithetic motif. R_{d_1} and R_{d_2} are dilution reactions with dilution rate γ, representing the dilution processes of control species Z_1 and Z_2. These two reactions are ignored in the previous design of aPID. With this, the BCRNs representation of the aPID with dilution processes is completed. Thus, the stoichiometric matrix S_{cl} and propensity function λ_{cl} of $\mathrm{N_{cl}}$ described in the right of Fig. 1. The control architectures can be obtained by suitably selecting the functions $g(\mu, x_n)$ and $h(z_1, x_1, x_n)$. A theoretical linear perturbation analysis is carried out in Section 2.3 to verify the proportional–integral–derivative control structure of the proposed controllers. In fact, the analysis applies to any smooth function $h(z_1, x_1, x_n)$ which is monotonically increasing (resp. decreasing) in z_1 (resp x_1 and x_n), and any smooth function $g(\mu, x_n)$ that is monotonically increasing (resp. decreasing) in μ (resp. x_n). The genetic implementation of the various control mechanisms presented throughout the paper can be carried out using basic activators, repressors and proteases which do not require any complicated biophysical mechanisms to implement the control designs. See Section 4 for more details on the genetic implementations.

2.3. Linear perturbation analysis

Considering an arbitrary plant controlled by an aPID controller described in Fig. 1, the dynamics of the closed-loop system, based on a common kinetic assumption —mass action kinetics, can be represented by a set of ordinary differential equations as

$$\begin{cases} \dot{x} = f(x) + h(z_1, x_1, x_n) e_1 \\ \dot{z}_1 = \mu + \beta x_n - \eta z_1 z_2 - \gamma z_1 \\ \dot{z}_2 = \theta x_n - \eta z_1 z_2 - \gamma z_2 \end{cases} \tag{1}$$

where $x := \begin{bmatrix} x_1 & x_2 & \cdots & x_n \end{bmatrix} \in \mathbb{R}^{n\times 1}$, $e_1 := \begin{bmatrix} 1 & 0 & \dots & 0 \end{bmatrix}^T \in \mathbb{R}^{n\times 1}$ and $f(x) := S\lambda(x)$. The perturbation from the fixed point $\begin{bmatrix} \bar{x}^T & \bar{z}_1 & \bar{z}_2 \end{bmatrix}^T$ of Eq. (1) should be denoted by $\begin{bmatrix} \tilde{x}^T & \tilde{z}_1 & \tilde{z}_2 \end{bmatrix}^T$. We assume that the reference signal μ is permitted to vary slightly in time around a nominal constant reference $\bar{\mu}$ in order to do a linear perturbation analysis. That is, we have

$$\begin{cases} \tilde{x}(t) = x(t) - \bar{x} \\ \tilde{z}_1(t) = z_1(t) - \bar{z}_1 \\ \tilde{z}_2(t) = z_2(t) - \bar{z}_2 \\ \tilde{\mu}(t) = \mu(t) - \bar{\mu} \end{cases} \tag{2}$$

Then the linearized dynamics can thus be written as

$$\begin{cases} \dot{\tilde{x}} = A\tilde{x} + \left(\sigma_1 \tilde{z}_1 - \sigma_2 \tilde{x}_1 - \sigma_3 \tilde{x}_n\right) e_1 \\ \dot{\tilde{z}}_1 = \tilde{\mu} + \beta \tilde{x}_n - \eta \bar{z}_1 \tilde{z}_2 - \eta \tilde{z}_1 \bar{z}_2 - \gamma \tilde{z}_1 \\ \dot{\tilde{z}}_2 = \theta \tilde{x}_n - \eta \bar{z}_1 \tilde{z}_2 - \eta \tilde{z}_1 \bar{z}_2 - \gamma \tilde{z}_2 \end{cases} \tag{3}$$

where the jacobians are defined as $A := \partial f(\bar{x})$, $\partial h(\bar{z}_1, \bar{x}_1, \bar{x}_n) =: \begin{bmatrix} \sigma_1 & -\sigma_2 & -\sigma_3 \end{bmatrix}$, and $\sigma_1, \sigma_2, \sigma_3 > 0$. Taking the laplace transforms of Eq. (3) and omitting irrelevant state variables yields

$$\tilde{x}_n(s) = {e_n}^T (sI - \bar{A})^{-1} e_1 \tilde{u}(s); \bar{A} := A - \sigma_2 e_1 e_1^T \tag{4}$$

$$\tilde{u}(s) = \sigma_1 \tilde{z}_1(s) - \sigma_3 \tilde{x}_n(s) \tag{5}$$

$$\tilde{z}_1(s) = \frac{\tilde{\mu}(s) + \beta \tilde{x}_n(s) - \eta \bar{z}_1 \tilde{z}_2(s)}{s + \eta \bar{z}_2 + \gamma} \tag{6}$$

$$\tilde{z}_2(s) = \frac{\theta \tilde{x}_n(s) - \eta \bar{z}_2 \tilde{z}_1(s)}{s + \eta \bar{z}_1 + \gamma} \tag{7}$$

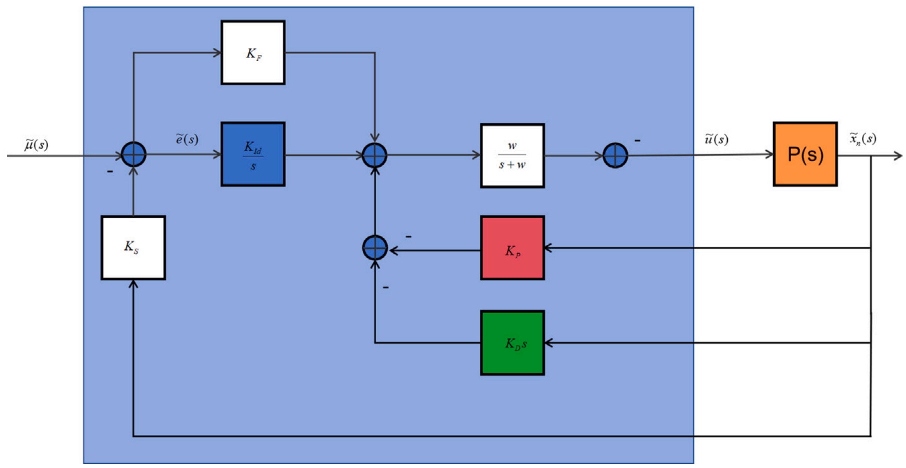

Fig. 2. Block diagram of the aPID feedback controllers without dilution.

Next, let $\tilde{z}_1(s)$ and $\tilde{z}_2(s)$ be represented by $\tilde{\mu}(s)$ and $\tilde{x}_n(s)$ respectively. The error defined as $\tilde{e}(s) := \tilde{\mu}(s) - (\theta - \beta)\tilde{x}_n(s)$. Then, Eqs. (6) and (7) can be rewritten as

$$\tilde{z}_1(s) = \frac{s}{D}\left[\tilde{\mu}(s) + \beta\tilde{x}_n(s) + \frac{\eta\bar{z}_1}{s}\tilde{e}(s) + \frac{\gamma E}{s}\right] \tag{8}$$

$$\tilde{z}_2(s) = \frac{s}{D}\left[\theta\tilde{x}_n(s) - \frac{\eta\bar{z}_2}{s}\tilde{e}(s) + \frac{\gamma\theta\tilde{x}_n(s)}{s}\right] \tag{9}$$

where $D := s^2+(\eta\bar{z}+2\gamma)s+\eta\bar{z}\gamma+\gamma^2$, $\bar{z} := \bar{z}_1(s)+\bar{z}_2(s)$, $E := \tilde{\mu}(s)+\beta\tilde{x}_n(s)$, substituting Eqs. (8) and (9) into Eq. (5), we obtain

$$\tilde{u}(s) = \left[\frac{\sigma_1}{\eta\bar{z}}\tilde{\mu}(s) + \frac{\bar{z}_1\sigma_1}{\bar{z}}\frac{\tilde{e}(s)}{s} + \frac{\sigma_1\beta}{\eta\bar{z}}\tilde{x}_n(s) + \frac{\gamma E}{s}\right]W - \sigma_3\tilde{x}_n(s) \tag{10}$$

where $W := \frac{\eta\bar{z}+\gamma}{s+\eta\bar{z}+\gamma} - \frac{\gamma}{s+\gamma}$. Eq. (10) provides an initial insight into the structure of the aPID controller N_c. Subsequently, the specific impact of the species dilution processes on the aPID control structure is further investigated. Specifically, The different forms of Eq. (10) corresponding to varying values of γ are examined. The discussion is presented below.

Case 1: When there is no dilution processes, i.e, R_{d_1}, R_{d_2} do not exist, $\gamma = 0$, thus Eq. (10) and closed-loop system N_{cl} can be written as

$$\begin{cases} \tilde{u}(s) = \Bigg[K_F\tilde{\mu}(s) + \dfrac{K_I}{s}\tilde{e}(s) \\ \quad - (K_P + K_D s)\tilde{x}_n(s) \Bigg] \dfrac{w}{s+w}; \\ \tilde{x}_n(s) = P(s)\tilde{u}(s). \end{cases} \tag{11}$$

where

$$\begin{cases} K_P = \sigma_3 - \dfrac{\sigma_1\beta}{\eta\bar{z}}, K_I = \sigma_1\dfrac{\bar{z}_1}{\bar{z}}, K_D = \dfrac{\sigma_3}{\eta\bar{z}}, \\ w = \eta\bar{z}, \\ P(s) = e_n^T(sI - \bar{A})^{-1}e_1, \\ \tilde{e}(s) = \tilde{\mu}(s) - K_S\tilde{x}_n(s), K_F = \dfrac{\sigma_1}{\eta\bar{z}}, K_S = \theta - \beta. \end{cases} \tag{12}$$

Eq. (11) provides the relationship between the biochemical reaction network parameters and the aPID controller parameters when the species dilution processes is absent in the aPID controller. In this case, the block diagram of the aPID controller's structure is depicted in Fig. 2. According to Eq. (12), it can be inferred that the P, I, D structures generated by IFEL and antithetic motif are inseparable. For instance, η simultaneously affects both K_D and K_P.

Case 2: When there are dilution processes, i.e, $\gamma > 0$, Eq. (10) and closed-loop system N_{cl} can be written as

$$\begin{cases} \tilde{u}(s) = \Bigg[K_{Fd}\tilde{\mu}(s) + K_{Id}\dfrac{\tilde{e}(s)}{s} + K_{Iu}\dfrac{\tilde{\mu}(s)}{s} \\ \quad - (K_{Pd} + K_{Dd}s)\tilde{x}_n(s) + K_{Ixn}\dfrac{\tilde{x}_n(s)}{s} \Bigg] W; \\ \tilde{x}_n(s) = P(s)\tilde{u}(s). \end{cases} \tag{13}$$

where

$$\begin{cases} K_{Pd} = \sigma_3 - \dfrac{\sigma_1\beta}{\eta\bar{z}} + \dfrac{2\sigma_3\gamma}{\eta\bar{z}}, \\ K_{Id} = \sigma_1\dfrac{\bar{z}}{\bar{z}}, K_{Dd} = \dfrac{\sigma_3}{\eta\bar{z}}, \\ K_{Ixn} = \dfrac{\sigma_1\beta\gamma}{\eta\bar{z}} - \sigma_3\gamma - \dfrac{\sigma_3\gamma^2}{\eta\bar{z}}, K_{Iu} = \dfrac{\sigma_1\gamma}{\eta\bar{z}}, \\ W = \dfrac{w_1}{s+w_1} - \dfrac{w_2}{s+w_2}, w_1 = \eta\bar{z}+\gamma, w_2 = \gamma, \\ P(s) = e_n^T(sI - \bar{A})^{-1}e_1, \\ \tilde{e}(s) = \tilde{\mu}(s) - K_S\tilde{x}_n(s), K_{Fd} = \dfrac{\sigma_1}{\eta\bar{z}}, K_S = \theta - \beta. \end{cases} \tag{14}$$

The expression Eq. (13) represents the linearized result of the aPID controller with dilution. It directly reveals the impact of the dilution processes on the structure of the aPID controller N_c, as shown in Fig. 3.

In comparison to Eq. (11), the proportional component in Eq. (13) is more intricate, with increased coupling between P, I and D terms. The low-pass filter $\frac{w}{s+w}$ has transformed to $\frac{w_1}{s+w_1} - \frac{w_2}{s+w_2}$, enabling the frequency f range from $\{f : f \leq \eta\bar{z}\}$ to $\{f : \gamma < f \leq \eta\bar{z}+\gamma\}$. Furthermore, it should be noted that in Eq. (13), there are two additional integral components, namely the integral term $K_{Iu}\frac{\tilde{\mu}(s)}{s}$ of the reference input $\tilde{\mu}(s)$ and the integral term $K_{Ixn}\frac{\tilde{x}_n(s)}{s}$ of the control output $\tilde{x}_n(s)$. These two integral components, which are absent in Eq. (11), arise due to the presence of the dilution processes in the control species.

In this section, the control structure Eq. (13) of the aPID controller with the dilution processes of the control species is derived using the linear perturbation method. From this control structure, it can be observed that the original structure Eq. (11) of the aPID controller is altered due to the presence of the dilution processes of the control species. As a result, the characteristics of the controller are also changed, such as the loss of the RPA property. In the numerical simulations conducted in Section 4, the influence of the dilution processes on the control performance can be visually observed. Subsequently, based on the obtained control structure Eq. (13), a new aPID controller is designed by constraining the reaction rate of the biochemical reaction in order to overcome the adverse effects caused by the dilution processes of the control species.

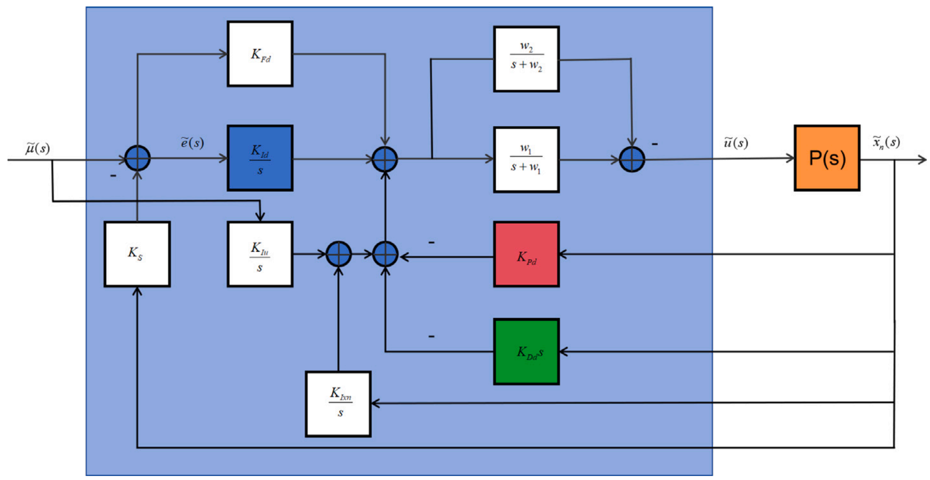

Fig. 3. Block diagram of the aPID feedback controllers with dilution.

3. Design and analysis of quasi-aPID

The goal of this section is to design an aPID controller with a dilution processes and exams its performance. The following analysis is based on two assumptions about the general controlled network. For convenience of description, let $F_i(i = 1, 2, \dots, n)$ represent the mapping between the system input u and the concentration of the controlled species x_i. When the system is stable, we have

$$\begin{cases} f(\bar{x}) + \bar{u}e_1 = 0 \\ \bar{x}_i = F_i(\bar{u}) = e_i^T \bar{x} \end{cases} \tag{15}$$

The two assumptions are described as follows.

Assumption 1. It is assumed that there always exists a valid input $\bar{u}$ that can achieve the desired steady-state output $\bar{x}_n = r$. More precisely, for $r > 0$, $\exists \bar{u} \in \Omega \subset \mathbb{R}$ such that $F_n(\bar{u}) = r$, where Ω represents the set of acceptable inputs for the controlled network.

Assumption 2. It is assumed that for a valid input $\bar{u}$, the steady-state concentration of the species $\bar{x}_i(i = 1, 2, \dots, n-1)$ in the plant N exists and is non-negative. That is, for $\bar{u} \in \Omega \subset \mathbb{R}$, $\exists \bar{x}_i \geq 0 (i = 1, 2, \dots, n-1)$ such that $\bar{x}_i = F_i(\bar{u})$.

It is significant to note that these two presumptions solely depend on the controlled network and the chosen driving input species; they are not reliant on the controller being utilized. If these presumptions are not met, the selection of input species will be inadequate. No controller could function if these presumptions could not be met since no kind of controller could provide the intended result without altering the concentration of the input species. For the sake of simplicity, we will assume $\Omega = \mathbb{R}_+$ in the analysis that follows.

3.1. Design of quasi-aPID

Next, let us consider the design of a class of aPID controllers with dilution processes, referred to as quasi-aPID controllers in this paper. In this controller, the inhibitory mechanism is degradation inhibition, the "driving" reactions R_a is equivalent to

$$Z_1 \longrightarrow Z_1 + X_1 \tag{16}$$

$$X_1 + X_n \longrightarrow X_n \tag{17}$$

The network module composed of Eqs. (16) and (17) generates a total propensity function $h(z_1, x_1, x_n) = kz_1 - \delta x_n \frac{x_1}{x_1+\kappa}$, representing the propensity function for the "driving" reactions. For a plant that satisfies Assumptions 1 and 2, when connected to a quasi-aPID controller, the dynamics of the closed-loop system can be represented as

$$\begin{cases} \dot{x} = S\lambda(x) + ue_1 \\ u = h(z_1, x_1, x_n) = kz_1 - \delta x_n \dfrac{x_1}{x_1 + \kappa} \\ \dot{z}_1 = \mu + \beta x_n - \eta z_1 z_2 - \gamma z_1 \\ \dot{z}_2 = \theta x_n - \eta z_1 z_2 - \gamma z_2 \end{cases} \tag{18}$$

When the closed-loop system is stable, $\dot{z}_1 = 0$, $\dot{z}_2 = 0$, thus the output of the closed-system is

$$\bar{x}_n = \frac{\mu - \gamma(\bar{z}_1 - \bar{z}_2)}{\theta - \beta} \tag{19}$$

If $\gamma = 0$, $\bar{x}_n =: r = \frac{\mu}{\theta - \beta}$, which is the set-point. It means the quasi-aPID should driven $\bar{x}_n$ to r.

According to Eq. (18), the equilibrium point $(\bar{z}_1, \bar{z}_2)$ of the controller can be represented as

$$\begin{cases} \bar{z}_1 = \dfrac{1}{k}[\bar{u} + \delta r \dfrac{\bar{x}_1}{\bar{x}_1 + \kappa}] \\ \bar{z}_2 = \dfrac{\mu + \beta r - \gamma \bar{z}_1}{\eta \bar{z}_1} \end{cases} \tag{20}$$

To ensure $\bar{z}_1, \bar{z}_2 \geq 0$, it should satisfy

$$\mu + \beta r \geq \gamma \bar{z}_1 \tag{21}$$

According to the definition of the partial derivatives in Eq. (4), we can obtain

$$\sigma_1 = k; \sigma_2 = \delta \bar{x}_n \frac{\kappa}{\left(\bar{x}_1 + \kappa\right)^2}; \sigma_3 = \frac{\delta \bar{x}_1}{\bar{x}_1 + \kappa} \tag{22}$$

Based on the analysis results in Section 2, we deal with the impacts brought by the dilution processes. To eliminate the integral term caused by the dilution processes, let $\eta \gg k\gamma$, then $K_{Iu} = \frac{k\gamma}{\eta \bar{z}} \rightarrow = 0$. To reduce the coupling between controller parameters, we denote $T(\bar{x}_1) := \frac{\bar{x}_1}{\bar{x}_1+\kappa}$ (When κ is sufficiently small, it approaches 1), and let $\eta \gg \gamma, \eta \gg \delta T(\bar{x}_1)\gamma, \eta \gg k\beta\gamma$. Meanwhile, to avoid the failure of the differential term due to excessive η, it is necessary to ensure $\delta T(\bar{x}_1) \gg \gamma$. According to Eq. (14), the gain and cutoff frequency of the controller can be obtained as

$$\begin{cases} K_{Pd} \approx \delta T(\bar{x}_1) - \dfrac{k\beta}{\eta \bar{z}}, K_{Id} = \dfrac{k\bar{z}_1}{\bar{z}}, K_{Dd} = \dfrac{\delta T(\bar{x}_1)}{\eta \bar{z}}, \\ w_1 \approx \eta \bar{z}, w_2 = \gamma, \\ K_{Fd} \approx 0, K_{Iu} \approx 0, K_{Ixn} \approx -\delta\gamma. \end{cases} \tag{23}$$

Clearly, the gain and cutoff frequency of the quasi-aPID controller depend on the specific controlled system. It can also be observed that the quasi-aPID controller includes an integral term not only for the error $\tilde{e}(s)$ but also for the system output $\tilde{x}_n(s)$.

Fixing κ, μ, r and thus $\bar{u}$ and $\bar{x}_1$, according Assumptions 1 and 2, and taking a small enough κ, then representing the biological molecule parameters $\eta, \delta, k, \beta, \theta$ in terms of gain and cutoff frequency in Eq. (23) results in the following

$$\begin{cases} \eta = \dfrac{K_{Id} w_1}{\bar{\mu} + rK_{Dd} w_1} \\ \delta = K_{Dd} w_1 \\ k^{\pm} \approx \dfrac{w_1}{2\mu}(\bar{u} + rK_{Pd} \\ \quad \pm \sqrt{(\bar{u} + rK_{Pd})^2 - 4\mu \dfrac{K_{Id}}{w_1}(\bar{u} + K_{Dd} w_1 r))} \\ \beta^{\pm} = \dfrac{w_1}{k^{\pm}} \left(K_{Dd} \omega_1 - K_{Pd} \right) \\ \theta^{\pm} = \dfrac{\mu}{r} + \beta^{\pm} \end{cases} \tag{24}$$

According to Eq. (24), it is evident that only an approximation of $k^{\pm}$ is obtained, as the processes of determining $k^{\pm}$ relies on condition $\eta \gg k\beta\gamma$. It should be noted that under this condition, the use of "≈" can be replaced with "=", and the impact on control performance can be neglected; this is merely for mathematical accuracy. Additionally, k, β, θ can be determined with two different sets of values to achieve the gain and cutoff frequency of quasi-aPID. However, it is important to highlight that the biological molecule parameters k, β, θ cannot be negative or complex, which restricts the range that quasi-aPID can cover in terms of gain and cutoff frequency. Now let us determine the parameter coverage range of quasi-aPID. Under the constraints of $\eta \gg \gamma$, $\eta \gg k\gamma$, $\eta \gg k\beta\gamma$, $\eta \gg \delta T(\bar{x}_1)$, $\delta T(\bar{x}_1) \gg \gamma$ and with the further restriction that k, β is a non-negative real number, the parameter coverage range of quasi-aPID is derived as follows

$$\begin{aligned} S = \{&(K_{Pd}, K_{Id}, K_{Dd}, w_1) \in \mathbb{R}^4 : \\ &K_{Pd} \le K_{Dd} w_1, \\ &0 \le K_{Id} < \frac{w_1}{4\mu} \frac{(\bar{u} + rK_{Pd})^2}{\bar{u} + K_{Dd}, w_1 r}, K_{Dd}, w_1 \ge 0\} \end{aligned} \tag{25}$$

Eq. (25) implies that it is possible to adjust the gain and control frequency within a certain range by appropriately modulating the molecular parameters $\eta, \delta, k, \beta, \theta$ of biochemical reaction networks. Next, we demonstrate how to adjust the molecular parameters of the controller in a general gene expression network to achieve different control performance.

3.2. Performance analysis of quasi-aPID

The aim of this part is to evaluate the performance of the quasi-aPID. let us consider a gene expression network controlled by quasi-aPID, and the controlled network is represented by the BCRNs as follows

$$\begin{aligned} &X_1 \xrightarrow{k_1} X_2 \\ &X_1 \xrightarrow{\gamma_1} \emptyset \\ &X_2 \xrightarrow{\gamma_2} \emptyset \end{aligned} \tag{26}$$

where X_1 is the input species, X_2 is the output species and k_1, γ_1, γ_2 are reaction rates. When connecting quasi-aPID to this controlled network, the dynamic model of the controlled network can be represented as follows

$$\begin{cases} \dot{x}_1 = u - \gamma_1 x_1 \\ \dot{x}_2 = k_1 x_1 - \gamma_2 x_2 \end{cases} \tag{27}$$

in which u represents the overall control input and x_2 is the system output, according to Eq. (27), the transfer function of the open-loop system can be obtained as follows

$$P(s) = \frac{k_1}{(s+\gamma_1)(s+\gamma_2)} \tag{28}$$

By using the control block diagram shown in Fig. 3, the transfer function of the closed-loop system can be obtained as follows

$$H(s) = \frac{(K_F s + K_I + K_{Iu})\Delta w k}{s^4 + p_3 s^3 + p_2 s^2 + p_1 s + p_0} \tag{29}$$

where

$$\begin{cases} p_0 = \gamma_1 \gamma_2 \gamma w_1 + K_I K_S k_1 \Delta w - K_{Ixn} k_1 \Delta w \\ p_1 = \gamma(\gamma_1 + \gamma_2) w_1 + \gamma_1 \gamma_2 (w_1 + \gamma) + K_P k_1 \Delta w \\ p_2 = \gamma w_1 + (\gamma_1 + \gamma_2)(w_1 + \gamma) + \gamma_1 \gamma_2 + k_1 \Delta w K_D \\ p_3 = w_1 + \gamma + \gamma_1 + \gamma_2 \\ \Delta w = w_1 - \gamma \end{cases} \tag{30}$$

Next, let us address the pole placement problem with the aim of determining the gain and cutoff frequency of quasi-aPID. To ensure system stability, the poles should be located in the left half of the complex plane and preferably on the real axis to prevent oscillations. Assuming that the closed-loop poles are situated at $s = -a$, theoretically, the larger the value of a, the faster the system response. Thus, the closed-loop characteristic polynomial is given by

$$p(s) = (s+a)^4 = s^4 + 4as^3 + 6a^2 s^3 + 4a^3 s + a^4 \tag{31}$$

To make $p(s)$ equal to the denominator of $H(s)$, quasi-aPID's gain and cutoff frequency can be expressed in terms of the controlled network parameters γ_1, γ_2, the control species dilution rate γ, and K_s as follows

$$\begin{cases} K_{Dd} = \dfrac{6a^2 - 4a(\gamma + \gamma_1 + \gamma_2)}{k_1(w_1 - \gamma)} \\ \quad + \dfrac{\gamma(\gamma_1 + \gamma_2) + (\gamma^2 + \gamma_1^2 + \gamma_2^2) + \gamma_1 \gamma_2}{k_1(w_1 - \gamma)} \\ K_{Pd} = \dfrac{4a^2 - \gamma(\gamma_1 + \gamma_2) w_1 - \gamma_1 \gamma_2 (w_1 + \gamma)}{k_1(w_1 - \gamma)} \\ K_{Id} = \dfrac{a^4 + K_{Dd} w_1 (w_1 - \gamma)\gamma - \gamma \gamma_1 \gamma_2 w_1}{K_S k_1 (w_1 - \gamma)} \\ w_1 = 4a - \gamma - \gamma_1 - \gamma_2 \end{cases} \tag{32}$$

Then, based on the controller parameter settings constraints given by Eq. (25), we seek to determine the range of poles on the real axis. While obtaining an analytical solution for the poles might not be possible, we can obtain a subset of the pole solution set, namely

$$\begin{aligned} &(K_{Pd}, K_{Id}, K_{Dd}, w_{c1}) \in S \\ &\Rightarrow \frac{\gamma_1 + \gamma_2}{2} \le a \le \gamma_1 + \gamma_2 \subset S_a \end{aligned} \tag{33}$$

where S_a represents the complete set of pole solutions. Starting from the obtained pole set, controller parameters K_{Dd}, K_{Pd}, K_{Id} are determined according to Eq. (32), followed by obtaining controller biochemical reaction network parameters δ, β, k via Eq. (24), resulting in the control of the system output x_2.

A gene expression network Eq. (26) controlled by quasi-aPID exhibits a range of pole values $\{a : -0.2 \le a \le -0.1\}$ when $\gamma_1 = 0.1$ and $\gamma_2 = 0.1$ as shown in Fig. 4a. These pole values correspond to different controller parameters, K_{Dd}, K_{Pd} and K_{Id} as represented in Fig. 4b, which in turn lead to variations in the biochemical reaction network parameters, k, δ and β as presented in Fig. 4c. The closed-loop system output x_2 is then observed in Fig. 4d for different combinations of controller's biochemical reaction network parameters. The pole set represents a subset of pole solutions, as obtaining the analytical solutions for all poles is not feasible due to practical physical limitations. Four values (−0.200, −0.167, −0.133, −0.100) are selected uniformly from the

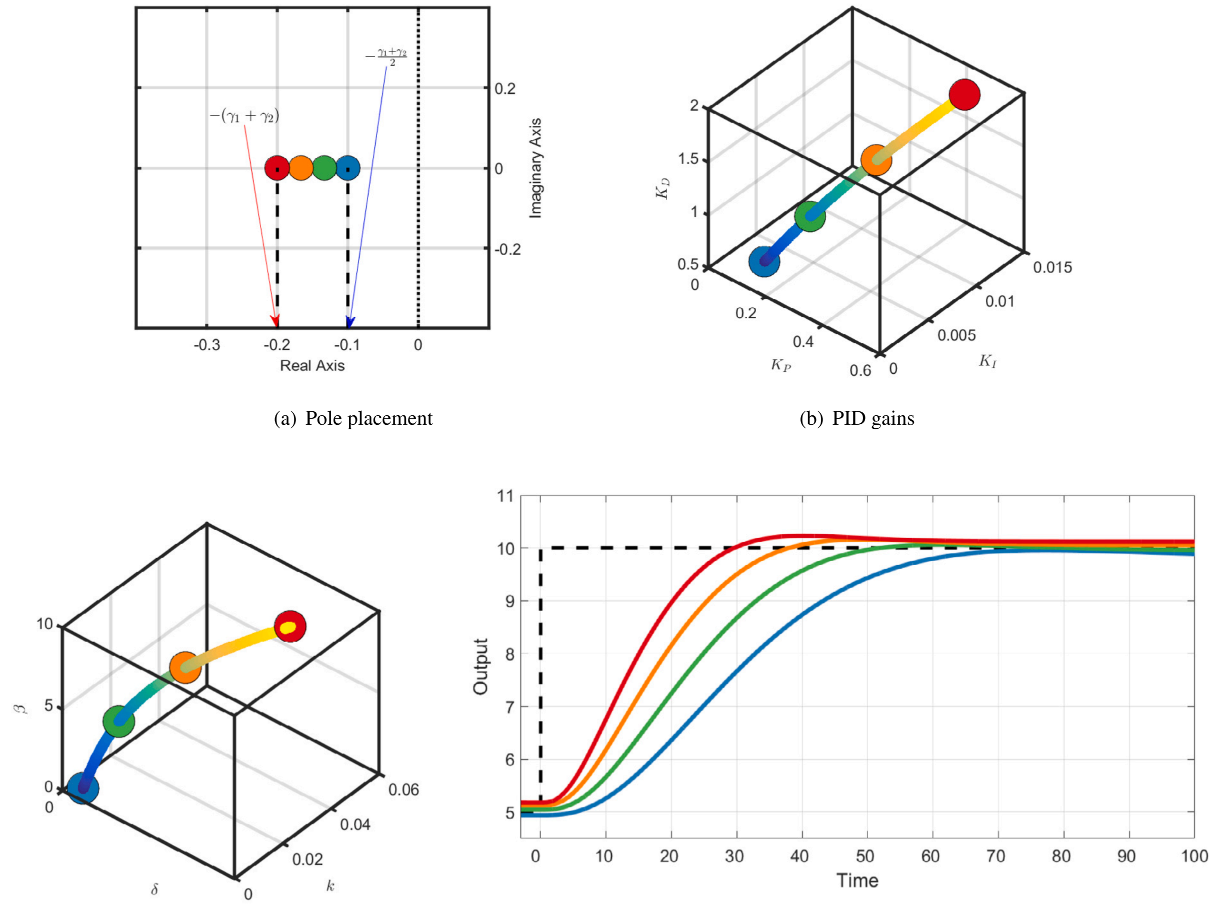

(a) Pole placement (b) PID gains

(c) Biomolecular parameters (d) Regulated system output

Fig. 4. Performance evaluation of quasi-aPID in a gene expression network model.

pole set to reflect the control performance of quasi-aPID. It is observed that as the pole values increase, the system response becomes faster.

In this section, the quasi-aPID is introduced, and the mapping between its biomolecular parameter spaces and the control structure is expressed through Eqs. (23) and (24). The range of coverage for controller parameters is defined by Eq. (25). The process of setting quasi-aPID's biomolecular parameters is demonstrated by controlling a gene expression model in Eq. (26). Additionally, two specific BCRNs from synthetic biology are utilized in the next section to further illustrate the characteristics of quasi-aPID.

4. Numerical simulation

This section validates the effectiveness of the quasi-aPID design through two numerical simulations, ensuring both RPA and enhanced dynamic performance. The gene expression of Escherichia coli and the whole body cholesterol metabolism model are examples of the regulated BCRNs. Furthermore, the 2nd order aPID controller proposed in [17] is chosen as a benchmark for comparison. The absolute value of steady-state error is chosen as the main performance metric, which reflects whether the controller guarantees RPA characteristics in the presence of external disturbances.

4.1. Regulation of gene expression in Escherichia coli

The performance of the quasi-aPID controller in a simulated basic network is the main topic of this part. With just two species, Escherichia coli's gene expression network is represented as the network under control.

Fig. 5 provides a comprehensive overview of the closed-loop system. The quasi-aPID controller involving Z_1 and Z_2, the disturbance network (see the right gray part of Fig. 5), and the plant (see the top of Fig. 5) compose the genetic closed-loop system. The goal is to force the regulated output X_2 to track an adjustable set-point. The implementation of the antithetic integral control involves the sequestration of the σ factor (SigW, represented by Z_1) and $anti-\sigma$ factor (RsiW, represented by Z_2), which are driven by P_{LUX} and P_{BAD}, respectively, as promoters. The expression rate μ of Z_1, which is adjustable with homoserine lactone (HSL), encrypts the set-point. There are two genes in a plant. The first gene is controlled by the SigW-responsive promoter PsigW and encodes exsA coupled to the degradation pdt tag (recognized by Mflon). The second gene, which encodes the transcription factor araC fused to the ssrA(DAS) degradation tag and the protease MfLon, is driven by the ExsA-responsive promoter PexsD. By expressing sspB at a tunable rate with anhydrotetracycline (aTc), the disturbance (see the right gray part of Fig. 5) speeds up the degradation rate of X_2. aTc identifies the DAS tag in X_2 and forwards it to the endogenous degradation machinery. While the AraC can activate both P_{BAD} and its lesser variant P_{BAD} (i.e., $\beta < \theta$), the MfLon in X_2 can degrade X_1. The integral control module is driven by the promoter P_{BAD}, whereas a second copy of a gene expressing $sigW$ is driven by P_{BAD}.

Then the BCRNs of the plant can be written as

$$
\begin{aligned}
&X_1 \xrightarrow{k_1} X_2 \\
&X_1 \xrightarrow{\gamma_1} \emptyset \\
&X_2 \xrightarrow{\gamma_2+\Delta} \emptyset
\end{aligned}
\tag{34}
$$

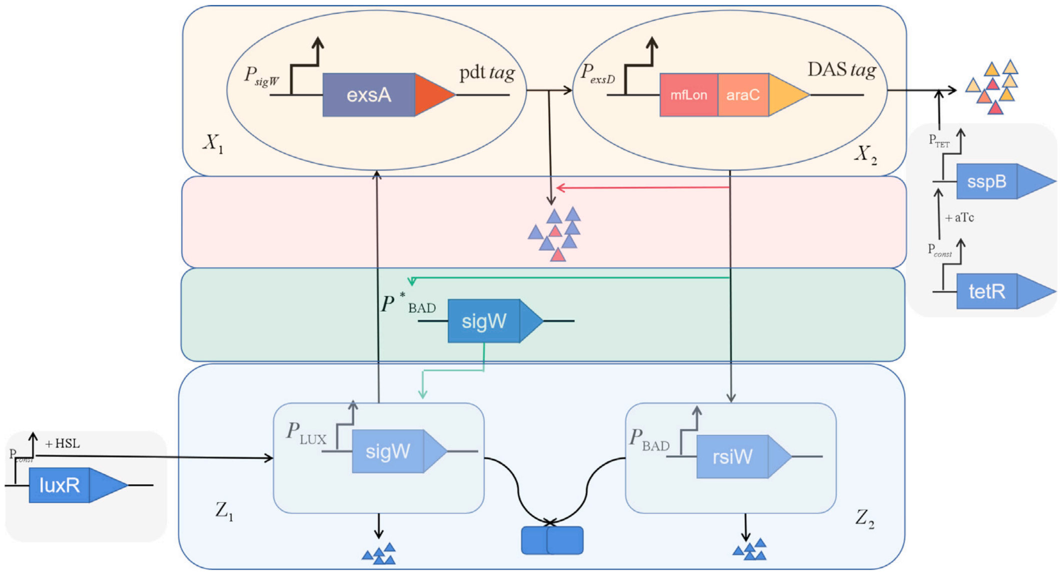

Fig. 5. Schematic diagram of a closed-loop system comprising a gene expression network of E. coli and quasi-aPID.

Table 2
The controller parameter settings of Fig. 6.

Biomolecular parameter	2nd order aPID	2nd order aPID + Quasi-integral control
μ (nM min^{-1})	100.00	1000.00
θ (min^{-1})	1.00	10.00
β (min^{-1})	0.00	0.00
η (min^{-1})	0.05	0.05
k (min nM^{-1})	0.05	0.05
κ (nM)	10.00	10.00
δ (min^{-1})	0.14	0.14
γ (min^{-1})	0.10	0.10

Table 3
The controller parameter settings of Fig. 7.

Biomolecular parameter	2nd order aPID	Quasi-aPID
μ (nM min^{-1})	100.00	1000.00
θ (min^{-1})	1.00	10.00
β (min^{-1})	0.00	0.00
η (min^{-1})	0.05	0.25
k (min nM^{-1})	0.05	0.30
κ (nM)	10.00	10.00
δ (min^{-1})	0.14	0.84
γ (min^{-1})	0.10	0.10

Table 4
The absolute steady-state error of quasi-aPID and 2nd order aPID under γ = 0.1 min^{-1}.

Controller	$\mu = 50$ nM	$\mu = 100$ nM	$\mu = 100$ nM, $\Delta = 0.084$ min^{-1}
Quasi-aPID	0.37	3.31	2.22
2nd order aPID [17]	5.09	5.07	19.54

where X_1 is the input species, X_2 is the output species, Δ is an unknown disturbance, and k_1, γ_1, γ_2 are reaction rates. The plant denoted by N_1. Its parameter settings are the same as those listed in Ref. Filo et al. [17]. Let Eqs. (16) and (17) replace R_a in N_c, we get the BCRNs of quasi-aPID, denoted by N_{qc}. The controller N_{qc} settings are configured correctly based on the suggested aPID controller architecture in Section 3.

The dynamic equations cased by N_1 and N_{qc} can be written as

$$\begin{cases} \dot{x}_1 = u - \gamma_1 x_1; u = kz_1 - \delta x_2 \dfrac{x_1}{x_1+\kappa_1} \\ \dot{x}_2 = k_1 x_1 - (\gamma_2 + \Delta)x_2 \\ \dot{z}_1 = \mu + \beta x_2 - \eta z_1 z_2 - \gamma z_1 \\ \dot{z}_2 = \theta x_2 - \eta z_1 z_2 - \gamma z_2 \end{cases} \tag{35}$$

According to Eq. (35), when the closed-system (N_1 and N_{qc}) is stable, the stable state of x_2 can be written as

$$\bar{x}_2 = \frac{\mu - \gamma(\bar{z}_1 - \bar{z}_2)}{\theta - \beta} \tag{36}$$

First, we use the quasi-integral control that is suggested in Ref. Qian and Del Vecchio [24]. Following this method, the parameter μ, θ, β is scaled by the same factor, such that $\mu \gg \gamma$, $\theta \gg \gamma$, $\beta \gg \gamma$. Consequently, Eq. (36) can be expressed as follows

$$\bar{x}_2 \approx \frac{\mu}{\theta - \beta} \tag{37}$$

From Eq. (37), it appears that quasi-integral control combined with 2nd order aPID can potentially achieve the desired trajectory tracking.

However, based on the simulation results shown in Fig. 6 (The controller parameter settings are shown in Table 2), the control output does not stabilize at the set-point. At the beginning, the reference signal μ is set to 50 nM. At the 8th hour, the reference signal is changed to 100 nM. At the 16th hour, a system disturbance is introduced. The blue line represents the system output under the control of the 2nd-aPID controller without dilution of control species. The green line represents the system output under the control of the 2nd order aPID controller with dilution of control species. It can be observed that the system output deviates from the set-point, both in tracking the step signal and in the presence of system disturbance. The red line represents the system output under the control of the quasi-aPID controller with dilution of control species while using quasi-integral control. The mismatch between quasi-integral control and aPID can be observed as it has not been able to achieve the desired trajectory tracking. Not only does the system output deviate from the set-point, but it may also exhibit oscillations. This phenomenon can be attributed to the degradation inhibition mechanism in the controller, which is not considered in quasi-integral control.

According to Section 3.1, it is crucial to ensure $\eta \gg k\beta\gamma$. Therefore, when β is multiplied by a factor, it is necessary to increase η correspondingly. This can result in a decrease in differential gain K_{Dd}, which may increase overshoot and cause oscillation. According to Eq. (23), increasing δ can increase K_{Dd}. However, δ is also positively related to K_{Pd} and negatively related to K_{Ixn}, where K_{Ixn} can be expressed in

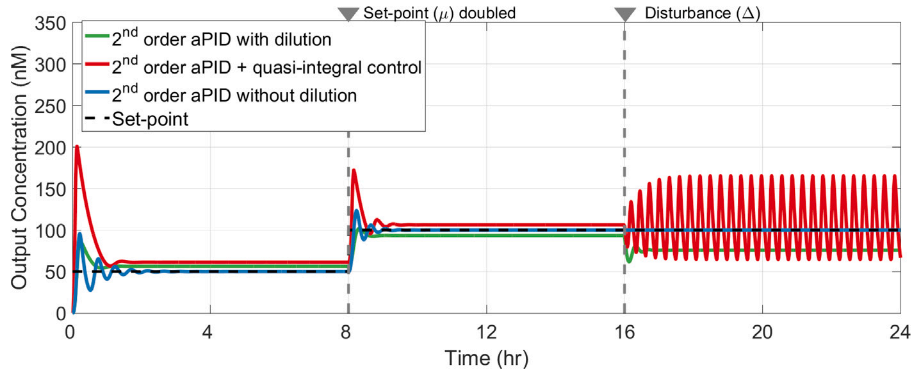

Fig. 6. The concentration of X_2 with 2nd order aPID [17] and quasi-integral control [24].

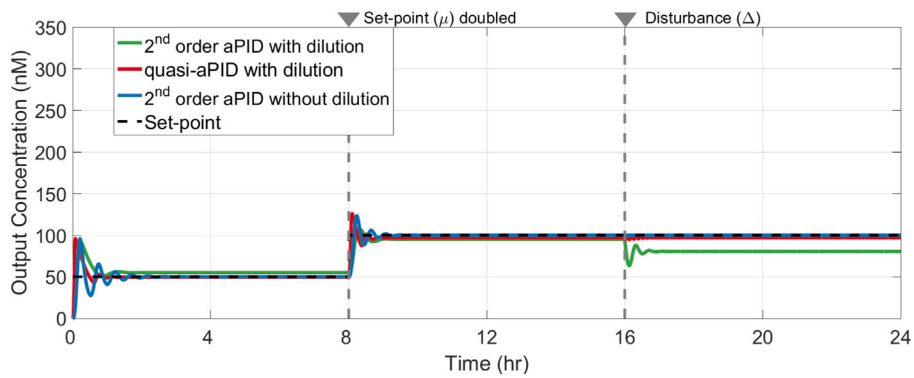

Fig. 7. The concentration of X_2 under the control of quasi-aPID.

terms of K_{Dd}. Therefore, the magnitude of increase in δ only needs to balance K_{Dd} and K_{Pd}. Following the quasi-aPID's parameter setup (The controller parameter settings are shown in Table 3), the control output (red line) in Fig. 7 is produced. It can be seen that the quasi-aPID controller achieves a similar control effect as the 2nd-aPID controller without dilution of control species, almost perfectly tracking the set-point and ensuring RPA. The corresponding absolute steady-state error is shown in Table 4. Clearly, the quasi-aPID exhibits a smaller absolute steady-state error.

4.2. Application of quasi-aPID in a whole body cholesterol metabolism model

This section examines the regulation of plasma cholesterol levels in the human body to illustrate the efficacy of quasi-aPID in managing intricate biochemical networks. Cardiovascular illnesses are largely caused by elevated cholesterol levels, especially low-density lipoprotein cholesterol (LDL-C). The natural regulatory systems of the human body regulate the amount of LDL-C in the blood. But as people age, these regulatory systems frequently deteriorate, which can cause metabolic problems and elevated LDL-C levels. As controlled network, use the whole body cholesterol metabolism model that is described in Ref. Mc Auley [33], as shown in Fig. 8.

The model monitors the circulation of cholesterol, including its different forms, throughout the body. In brief, Intestinal Cholesterol (IC) originates from the daily dietary intake or is secreted by the liver (Hepatic Tissue) through biliary secretion. Additionally, the intestine itself synthesizes IC. The fate of IC involves either excretion from the body or absorption and transportation to the liver, where it is subsequently released into the plasma via Very-Low-Density Lipoproteins (VLDL). Any excess cholesterol in peripheral tissues is transferred to the liver by High-Density Lipoproteins (HDL). Two external disturbances: a 304 mg/day increase in dietary intake (denoted by disturbance1) and a 25% increase in absorption (denoted by disturbance2). The former represents a shift in daily diet, while the latter pertains to higher intestinal absorption efficiency. When no feedback control is applied, both disturbances lead to an increase in cholesterol levels in the plasma. In the context of quasi-aPID control implementation, Intestinal Cholesterol (IC) is designated as the actuated input species, with Z_1 producing IC while the output species, LDL-C, degrades IC.

This cholesterol network has 43 parameters and 34 state variables (species), all of which are set to the same values as in Ref. Filo et al. [17]. LDL-C levels are controlled to keep at 100 mg/dL under these perturbations by connecting the quasi-aPID controller to this network, attaining RPA. The control species' dilution is taken into consideration as a result of deterioration, or as dictated by the control species' rate of degradation.

First, as Fig. 9a illustrates, the output species LDL-C concentration varied in response to disturbances when the regulated species' degradation rate is set to 0 (The controller parameter settings are shown in Table 5). It is evident that under the two previously described perturbations, the content of LDL-C considerably rises in the absence of aPID control (black line). The predicted control impact is demonstrated by both 2nd order aPID control and quasi-aPID control, guaranteeing RPA.

Taking into account the deterioration of the control species (The controller parameter settings are shown in Table 6), Fig. 9b illustrates how the 2nd order aPID controller encounters disturbance 2 (pink dashed line) and is unable to sustain RPA. Conversely, a quasi-aPID controller guarantees RPA with a negligible overshoot. The absolute steady-state error of quasi-aPID and 2nd order aPID is presented in Table 7. When disturbances are introduced, the absolute static error of quasi-aPID is significantly smaller compared to 2nd order aPID.

5. Conclusion

This work examines how species dilution affects the structure of the aPID controller through the linear perturbation method and devises

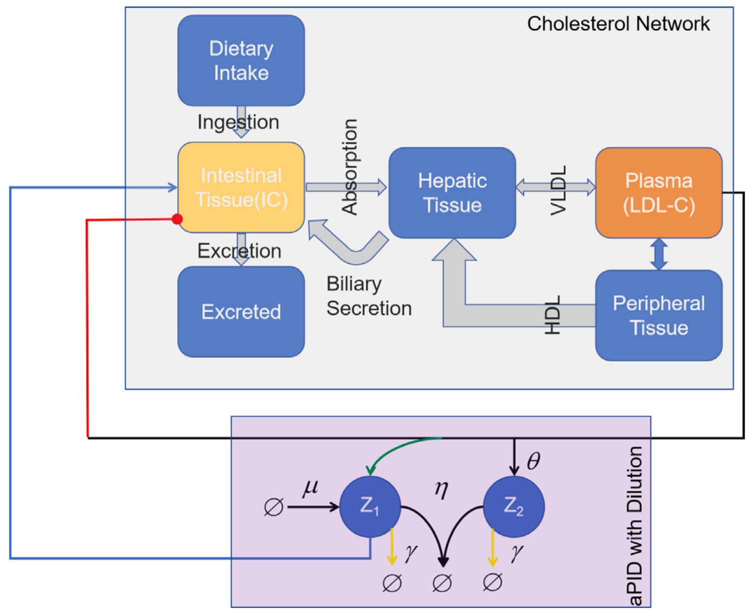

Fig. 8. Quasi-aPID control of a whole-body of cholesterol metabolism model.

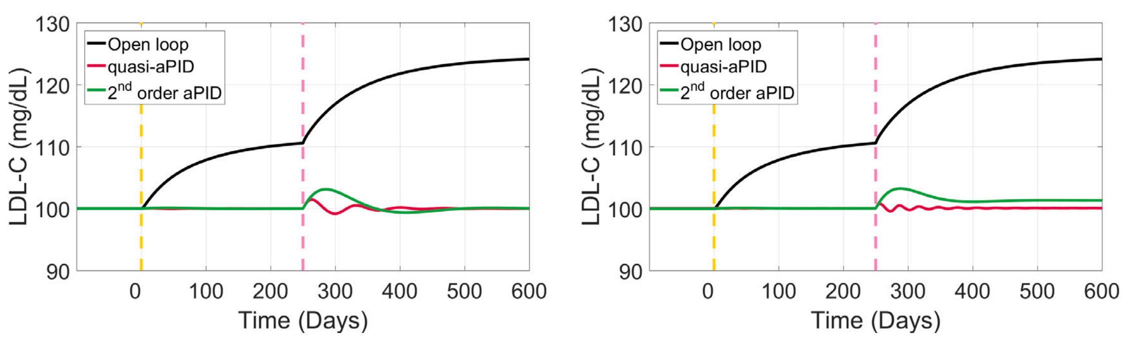

(a) The concentration of LDL-C with $\gamma = 0$

(b) The concentration of LDL-C with $\gamma = 0.01 min^{-1}$

Fig. 9. Comparison of concentration variations in LDC-C under the quasi-aPID and 2nd order aPID [17].

Table 5
The controller parameter settings of Fig. 9(a).

Biomolecular parameter	2nd order aPID	Quasi-aPID
μ (nM min^{-1})	100.00	1000.00
θ (min^{-1})	51.00	60.00
β (min^{-1})	50.00	50.00
η (min^{-1})	0.10	0.10
k (min nM^{-1})	100.00	100.00
κ (nM)	0.00	0.00
δ (min^{-1})	0.10	0.10
γ (min^{-1})	0.00	0.00

Table 6
The controller parameter settings of Fig. 9(b).

Biomolecular parameter	2nd order aPID	Quasi-aPID
μ (nM min^{-1})	100.00	1000.00
θ (min^{-1})	51.00	60.00
β (min^{-1})	50.00	50.00
η (min^{-1})	0.10	0.10
k (min nM^{-1})	100.00	100.00
κ (nM)	0.00	0.00
δ (min^{-1})	0.10	0.10
γ (min^{-1})	0.01	0.01

effective strategies to address the resulting detrimental effects. Subsequently, a novel aPID controller, referred to as quasi-aPID, is proposed.

Table 7
The absolute steady-state error of quasi-aPID and 2nd order aPID under $\gamma = 0.01$ min^{-1}.

Controller	Disturbance1	Disturbance1 + Disturbance2
Quasi-aPID	0.01	0.04
2nd order aPID [17]	0.01	1.31

By designing the biochemical reaction rate of this controller, the adverse effects of the dilution processes on the aPID controller are reduced or even eliminated without the need for additional control species or reactions. Detailed performance analysis of the quasi-aPID controller is presented, along with the coverage range of its parameters. The controller is then applied to models of gene expression in Escherichia coli and whole-body cholesterol metabolism, and its effectiveness is demonstrated through numerical simulations. The simulation results show that quasi-aPID maintains the RPA. Meanwhile, regardless of the presence of external disturbances, quasi-aPID reduces the absolute value of steady-state error. In the future, the design of aPID will be further investigated to build high-performance controllers for the reliable manipulation of gene circuits in synthetic biology.

Funding

This work is supported by 111 Project of China (No. D23006), the National Natural Science Foundation of China (Nos. 62272079, 61972266), the Artificial Intelligence Innovation Development Plan Project of Liaoning Province (Nos. 2023JH26/10300025), the Natural Science Foundation of Liaoning Province (Nos. 2022-KF-12-14), the Scientific Research Fund of Liaoning Provincial Education Department (No. LJKZZ20220147), the Scientific Research Platform Project of Dalian University (No. 202301YB02), the State Key Laboratory of Synthetical Automation for Process Industries, the Postgraduate Education Reform Project of Liaoning Province (No. LNYJG2022493), the Dalian Outstanding Young Science and Technology Talent Support Program (No. 2022RJ08).

CRediT authorship contribution statement

Xun Deng: Writing – original draft, Validation, Methodology, Formal analysis. **Hui Lv:** Writing – review & editing, Supervision, Funding acquisition, Conceptualization. **Qiang Zhang:** Supervision, Funding acquisition. **Edmund Ming Kit Lai:** Supervision, Methodology.

Declaration of competing interest

The authors declare the following financial interests/personal relationships which may be considered as potential competing interests: Hui Lv reports article publishing charges was provided by National Natural Science Foundation of China. If there are other authors, they declare that they have no known competing financial interests or personal relationships that could have appeared to influence the work reported in this paper.

References

[1] M.E. Kotas, R. Medzhitov, Homeostasis, inflammation, and disease susceptibility, Cell 160 (5) (2015) 816–827.
[2] R. Mullur, Y.-Y. Liu, G.A. Brent, Thyroid hormone regulation of metabolism, Physiol. Rev. 94 (2) (2014) 355–382.
[3] M.H. Khammash, Cybergenetics: Theory and applications of genetic control systems, Proc. IEEE. Inst. Electr. Electron. Eng. 110 (5) (2022) 631–658.
[4] D.K. Agrawal, R. Marshall, V. Noireaux, E.D. Sontag, In vitro implementation of robust gene regulation in a synthetic biomolecular integral controller, Nature Commun. 10 (1) (2019) 5760.
[5] H. Chen, J. Fraser Stoddart, From molecular to supramolecular electronics, Nat. Rev. Mater. 6 (9) (2021) 804–828.
[6] A.H. Ng, T.H. Nguyen, M. Gómez-Schiavon, G. Dods, R.A. Langan, S.E. Boyken, J.A. Samson, L.M. Waldburger, J.E. Dueber, D. Baker, et al., Modular and tunable biological feedback control using a de novo protein switch, Nature 572 (7768) (2019) 265–269.
[7] R. Vogt, A. Guzman, C. Charron, L. Muñoz, Controllability and state feedback control of a cardiac ionic cell model, Comput. Biol. Med. 139 (2021) 104909.
[8] C. Barajas, D. Del Vecchio, Synthetic biology by controller design, Curr. Opin. Biotechnol. 78 (2022) 102837.
[9] T. Frei, C.-H. Chang, M. Filo, A. Arampatzis, M. Khammash, A genetic mammalian proportional–integral feedback control circuit for robust and precise gene regulation, Proc. Natl. Acad. Sci. USA 119 (00) (2022) e2122132119.
[10] C. Briat, A. Gupta, M. Khammash, Antithetic integral feedback ensures robust perfect adaptation in noisy biomolecular networks, Cell Syst. 2 (1) (2016) 15–26.
[11] M.H. Khammash, Perfect adaptation in biology, Cell Syst. 12 (6) (2021) 509–521.
[12] A. Gupta, M. Khammash, Universal structural requirements for maximal robust perfect adaptation in biomolecular networks, Proc. Natl. Acad. Sci. USA 119 (43) (2022) e2207802119.
[13] R. Vilanova, A. Visioli, PID Control in the Third Millennium, Springer, London, 2012.
[14] R.P. Borase, D. Maghade, S. Sondkar, S. Pawar, A review of PID control, tuning methods and applications, Int. J. Dyn. Control 9 (2021) 818–827.
[15] J. Bhookya, M.V. Kumar, J.R. Kumar, A.S. Rao, Implementation of PID controller for liquid level system using mGWO and integration of IoT application, J. Ind. Inf. Integr. 28 (2022) 100368.
[16] M. Babaei, T.M. Evers, F. Shokri, L. Altucci, E.C. de Lange, A. Mashaghi, Biochemical reaction network topology defines dose-dependent drug–drug interactions, Comput. Biol. Med. 155 (2023) 106584.
[17] M. Filo, S. Kumar, M. Khammash, A hierarchy of biomolecular proportional-integral-derivative feedback controllers for robust perfect adaptation and dynamic performance, Nature Commun. 13 (1) (2022) 2119.
[18] C. Briat, C. Zechner, M. Khammash, Design of a synthetic integral feedback circuit: dynamic analysis and DNA implementation, ACS Synth. Biol. 5 (10) (2016) 1108–1116.
[19] S.K. Aoki, G. Lillacci, A. Gupta, A. Baumschlager, D. Schweingruber, M. Khammash, A universal biomolecular integral feedback controller for robust perfect adaptation, Nature 570 (7762) (2019) 533–537.
[20] C.C. Samaniego, E. Franco, Ultrasensitive molecular controllers for quasi-integral feedback, Cell Syst. 12 (3) (2021) 272–288.
[21] N.M. Paulino, M. Foo, J. Kim, D.G. Bates, PID and state feedback controllers using DNA strand displacement reactions, IEEE Control Syst. Lett. 3 (4) (2019) 805–810.
[22] M. Whitby, L. Cardelli, M. Kwiatkowska, L. Laurenti, M. Tribastone, M. Tschaikowski, PID control of biochemical reaction networks, IEEE Trans. Automat. Control 67 (2) (2021) 1023–1030.
[23] S. Anastassov, M. Filo, C.-H. Chang, M. Khammash, A cybergenetic framework for engineering intein-mediated integral feedback control systems, Nature Commun. 14 (1) (2023) 1337.
[24] Y. Qian, D. Del Vecchio, Realizing 'integral control'in living cells: how to overcome leaky integration due to dilution? J. R. Soc. Interface 15 (139) (2018) 20170902.
[25] M. Chevalier, M. Gómez-Schiavon, A.H. Ng, H. El-Samad, Design and analysis of a proportional-integral-derivative controller with biological molecules, Cell Syst. 9 (4) (2019) 338–353.
[26] S. Modi, S. Dey, A. Singh, Proportional and derivative controllers for buffering noisy gene expression, in: Proc. IEEE 58th Conf. Decis. Control, 2019, pp. 2832–2837.
[27] J. Puchałka, A.M. Kierzek, Bridging the gap between stochastic and deterministic regimes in the kinetic simulations of the biochemical reaction networks, Biophys. J. 86 (3) (2004) 1357–1372.
[28] M. Tena-Solsona, C. Wanzke, B. Riess, A.R. Bausch, J. Boekhoven, Self-selection of dissipative assemblies driven by primitive chemical reaction networks, Nature Commun. 9 (1) (2018) 2044.
[29] Z.-Y. Sun, K. Zhang, C.-C. Chen, Q. Meng, Robust output feedback control of time-delay nonlinear systems with dead-zone input and application to chemical reactor system, Nonlinear Dynam. 109 (3) (2022) 1617–1627.
[30] X. Zhao, X. Wang, Y. Su, S. Unar, Network dynamics of a periodically forced chemical system and its application for tuning PID controller with time-delay systems, Nonlinear Dynam. (2023) 1–17.
[31] Y. Yuan, H. Lv, Q. Zhang, DNA strand displacement reactions to accomplish a two-degree-of-freedom PID controller and its application in subtraction gate, IEEE Trans. Nanobiosci. 20 (4) (2021) 554–564.
[32] N. Pachauri, J. Yadav, A. Rani, V. Singh, Modified fractional order IMC design based drug scheduling for cancer treatment, Comput. Biol. Med. 109 (2019) 121–137.
[33] M.T. Mc Auley, Effects of obesity on cholesterol metabolism and its implications for healthy ageing, Nutr. Res. Rev. 33 (1) (2020) 121–133.